ACS OMEGA

Open Access

http://pubs.acs.org/journal/acsodf

Article

Incompatibility of Pure SnO_2 Thin Films for Room-Temperature Gas Sensing Application

Anju Thomas, Logu Thirumalaisamy, Sridharan Madanagurusamy, and Kalainathan Sivaperuman*

Cite This: *ACS Omega* 2023, 8, 32848−32854

Read Online

ACCESS | Metrics & More | Article Recommendations | Supporting Information

ABSTRACT: Despite the high sensitivity and selectivity, the high operating temperature required for activation energy of tin oxide (SnO_2) still stands as a drawback for SnO_2 based gas sensors. In this work, the SnO_2 thin films were deposited through spray pyrolysis and were subjected to gas sensing at 27 °C (room temperature) towards different gases. The films exhibited a consistently low response of approximately 1 when tested to various VOCs. The type, concentration, and mobility of charge carriers were determined from the Hall measurements. The high carrier concentration accompanied by poor mobility and grain boundary scattering is supposed to hinder its performance at room temperature. The obtained film had spherical morphology, which lead to grain boundary scatterings and decreased the mobility of carriers.

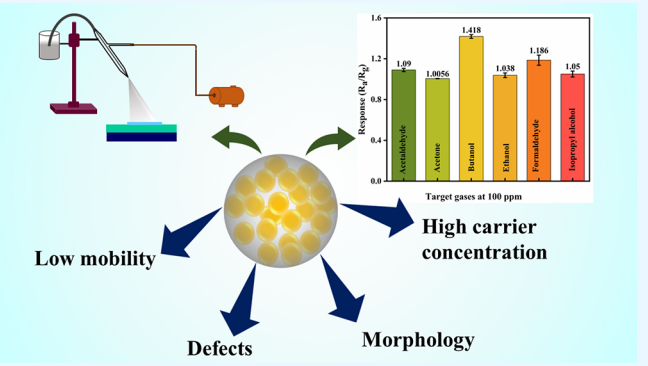

1. INTRODUCTION

The fast-growing industrialization and technological advancements have led to increased emissions of toxic gases including volatile organic compounds (VOCs) into the atmosphere. This causes serious health issues.[1] The electronic configuration and feasible electrical and morphological properties of metal oxides make them more suitable for gas sensor applications.[2] A sensor that uses the change in resistance as the means to detect the presence and concentration of target gas is the chemi-resistive gas sensor.[3,4] Tin oxide (SnO_2) is a functional material with high conductivity and optical transparency.[5] Hence, it finds a lot of applications in various fields of science and engineering. It is an n-type semiconductor with high melting point and a tetragonal rutile structure.[6] SnO_2 exhibits excellent thermoelectric properties and has been explored as a thermoelectric material.[7,8] SnO_2 stands as a good candidate for transparent conducting electrodes.[9,10] It is used as a catalyst to control the emission of CO and CH_4 due to surface oxygen deficiency and surface properties.[6,11] SnO_2 is a widely used sensing material for the detection of VOCs.[12,13] But they mostly operate at high temperatures (100−550 °C).[12,14−17] The operating temperature is provided to supply the activation energy to SnO_2. The contemporary available sensors require a heating unit to give the operating temperature to the sensing layer. This increases the cost of fabrication, increases the size of sensor units, affects the durability and stability of the sensor, requires purging, and limits its outreach.[18] Thus, room-temperature gas sensors are anticipated recently for commercialization and real-time applications. This article discusses the deposition of SnO_2 thin films using the chemical spray pyrolysis method. The gas sensing of the deposited films was carried out at 27 °C. The incompatibility of synthesized SnO_2 thin films being used as a chemi-resistive gas sensor at 27 °C is further discussed with the support of electrical and morphological studies.

The SnO_2 thin film was synthesized using the chemical spray pyrolysis method. This is a promising technique to generate crystalline and uniform thin films even for large-scale fabrication of devices. In the spray pyrolysis technique, the precursor solution is sprayed onto the heated substrates, where the solution undergoes a decomposition reaction and the required compound is formed on the substrate as a thin film.[19] The first step is the precursor solution preparation, where the precursors are selected such that a clear stable solution is obtained and the byproducts are volatile. The next is the generation of aerosols, which was achieved by nebulizer spray, followed by the transport of these aerosols to the substrate.[20] In this step, the nozzle-to-substrate distance, spray angle, spray time, spray interval, substrate temperature, etc., play a significant role in the formation of different morphologies, textures, and crystallinity of the thin film. At the final stage, the aerosols decompose, nucleate, and coalesce together, leading to the formation of a thin film.

Received: June 8, 2023
Accepted: August 8, 2023
Published: August 30, 2023

2. EXPERIMENTAL SECTION

2.1. Thin-Film Synthesis. The thin films of SnO_2 were deposited on glass substrates through the chemical spray pyrolysis method using a home-made setup reported elsewhere.[21] The illustration of the spray pyrolysis setup is given in Figure 1. The precursor used was tin(II) chloride ($SnCl_2 \cdot 2H_2O$) (Sigma-Aldrich). Forty milliliters of double-distilled (DD) water was used as the solvent. Two milliliters of HCl was added into the solution with constant stirring to prepare a stable homogeneous solution. The prepared clear transparent precursor solution was then sprayed onto the properly cleaned soda lime glass with the nozzle-to-substrate distance of 30 cm, nozzle diameter of 0.4 mm, spray time of 10 s, and spray interval of 90 s using compressed air as the carrier gas. The effect of substrate temperature and molarity of precursor solution was studied by varying them from 250 to 300 °C and 0.025 to 0.2 M, respectively.

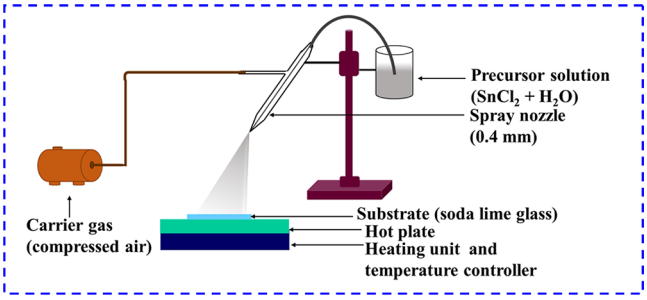

Figure 1. Schematic diagram of the spray pyrolysis setup.

2.2. Characterizations. The thin films were subjected to XRD (Bruker D8 Advance, Germany), UV−visible spectroscopy (JASCO V-670 PC), AFM (NaioAFM 60-14-080), Hall measurements, FE-SEM (Thermo Fisher FEI QUANTA 250 FEG), and EDX mapping (Oxford Instruments) studies. The gas sensing studies were carried out using a home-made gas sensing setup given elsewhere.[1] Thin films with 1.5 cm length and 1.5 cm breadth were taken as the sensing layer. Ohmic contacts were made on the surface of the sensing layer using zero resistance copper wire and highly conducting silver paste. This was then connected to the Keithley electrometer 6517 B, which was interfaced to a desktop. Initially, the setup was left undisturbed to attain a steady baseline resistance. Then after, target gas was injected into the chamber through the inlet and the corresponding changes in resistance was measured. The schematic diagram of the sensing setup is shown in Figure 2. The sensor response was calculated[22] as

$$S = \frac{R_a}{R_g} \tag{1}$$

where R_a and R_g are the resistance in the absence and presence of target gas, respectively.[23] Response time is the time taken by the sensor to reach 90% of its final value in the presence of target gas. Recovery time is the time taken by the sensor to reach 10% of the initial value on the removal of target gas.[24] The target gas concentration in the chamber was calculated using the formula[1,21,25−27]

$$C_{ppm} = \frac{\rho \times R \times V_l \times T \times 10^6}{V_c \times MW \times P} \tag{2}$$

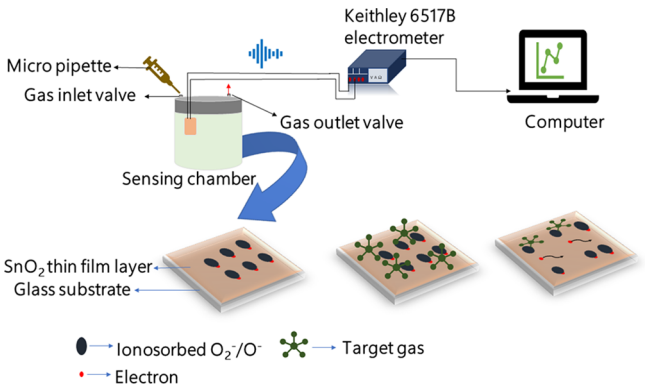

Figure 2. Schematic diagram of the sensing setup.

where V_l is the volume of liquid gas, C_{ppm} is the concentration of gas, MW is the molecular weight of gas, V_c is the volume of the chamber, P_c is the pressure inside the chamber, which is 1 atm, ρ is the density of gas, R is the ideal gas constant, and T is the temperature of the chamber.

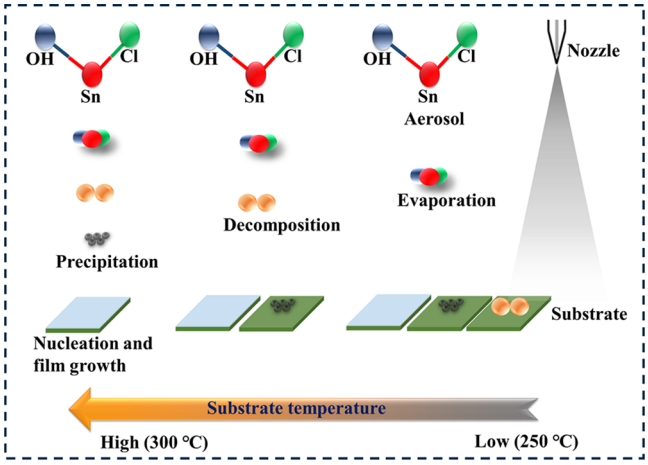

Figure 3. Schematic diagram for processes involved in spray pyrolysis under different temperature conditions.

3. RESULTS AND DISCUSSION

The XRD patterns of SnO_2 thin films at different molarities with a substrate temperature of 300 °C are given in Figure 4a. The dependence of substrate temperature for 0.1 M is studied, and the corresponding XRD patterns are shown in Figure 4b. The JCPDS card file number 01-077-0447 was used as the reference file for all the films. From XRD, a rutile structure with a tetragonal unit cell was confirmed for all films. The crystallite size for the films was found using the Debye Scherrer formula.[28]

$$D = \frac{0.9\lambda}{\beta \cos\theta} \tag{3}$$

The lattice strain of the films was also found from XRD using the formula[29]

$$\varepsilon = \frac{\beta \cos\theta}{4} \tag{4}$$

It is also clear that 0.025 M films were little amorphous when compared to the other films. This is because, at lower

https://doi.org/10.1021/acsomega.3c04038
ACS Omega 2023, 8, 32848−32854

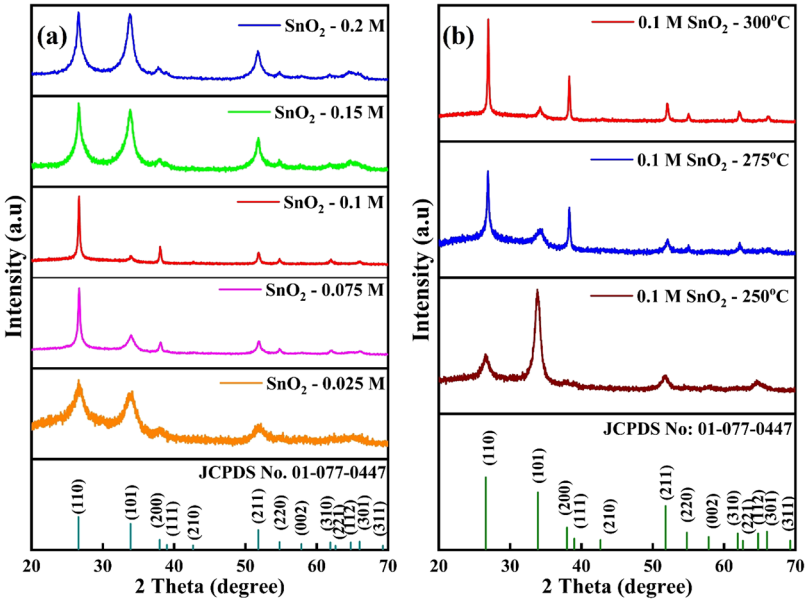

Figure 4. (a) XRD pattern of SnO_2 thin films with different molarities deposited at 300 °C and (b) XRD pattern of SnO_2 samples with 0.1 M at different deposition temperatures.

Table 1. Inferences from XRD

sample	0.1 M, 300 °C (S1)	0.1 M, 275 °C	0.1 M, 250 °C	0.025 M, 300 °C	0.075 M, 300 °C	0.15 M, 300 °C	0.2 M, 300 °C
crystallite size (nm)	88.96	32	45.46	27.83	34.3	65.4	19.73
lattice strain (%)	0.25	0.61	0.29	0.49	0.35	0.21	0.62
a (Å)	4.73	4.70	4.74	4.73	4.72	4.75	4.75
C (Å)	2.85	3.15	3.12	3.16	3.19	3.19	3.19

concentrations, the number of nucleation sites is less due to lower amount of Sn. When the concentration of Sn increases, the nucleation sites also increase; hence, more crystalline films are achieved.[30] The intensity of the peak corresponding to (101) decreases on increasing the molarity from 0.025 to 0.1 M. Then, there is a rapid increase in the peak intensity as the molarity is further increased to 0.15 and 0.2 M. It was observed that, as the substrate temperature increases from 250 to 300 °C, the intensity of peak corresponding to (110) increases and that corresponding to (101) decreases. The crystallinity of the film also increased with an increase in substrate temperature. This might be due to insufficient thermal energy to complete the oxidation process of Sn at low temperatures. As the temperature is increased, Sn oxidizes completely and more crystalline films are achieved.[31−33] Furthermore, there is growth in the (200) direction as the substrate temperature increases. The schematic diagram representing the processes happening in the deposition of the thin film through spray pyrolysis under different temperature conditions (low to high) is given in Figure 3. For the further studies in this work, a 0.1 M sample deposited at 300 °C was used and termed as S1, as it was more crystalline and had larger crystallite size. Moreover, this sample had an orientation along (110). The (110) surface of SnO_2 is considered to be the stable face of naturally grown SnO_2.[34,35] The average crystallite size, strain, and lattice constants of the films are given in Table 1.

The gas sensing capabilities of the SnO_2 thin films (S1) were studied at 27 °C toward 100 ppm of ethanol, acetone, isopropyl alcohol, acetaldehyde, formaldehyde, and butanol. Unfortunately, for all gases, the sensor response was almost the same (∼1), as given in Figure 5. The response and recovery of

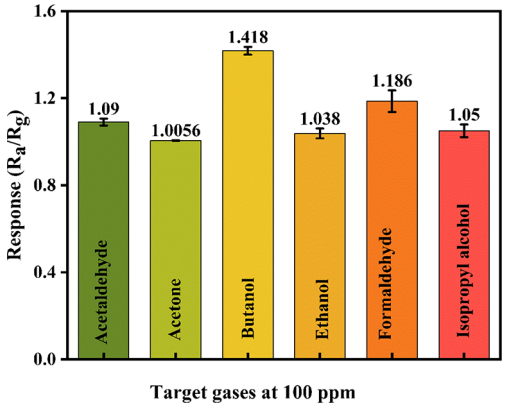

Figure 5. Responsiveness of the S1 sample toward various gases tested at 100 ppm at 27 °C.

each of these gases are given in Figure 7. The sensing responses were repeated for five cycles to study the repeatability of the results, and they are given in Figure 6a. The average response values recorded were 1.09, 1.00, 1.42, 1.04, 1.19, and 1.03 for acetaldehyde, acetone, butanol, ethanol, formaldehyde, and isopropyl alcohol, respectively. The sensor response for different concentrations (50 to 300 ppm) of formaldehyde and butanol was also studied.

It was noted that the sensor response had a very little increment when the concentration of target gases was increased. The response with an increase in target gas is demonstrated in Figure 6b. But still, the response of the sensor was around ∼1. Despite the result that response and recovery times for all gases were fast, the same response value

https://doi.org/10.1021/acsomega.3c04038
ACS Omega 2023, 8, 32848−32854

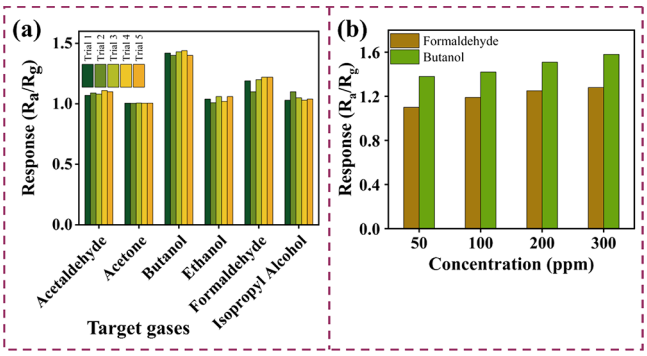

Figure 6. (a) Repeatability of the sensor response of S1 toward various target gases at 100 ppm and (b) sensor response of S1 to various concentrations of formaldehyde and butanol.

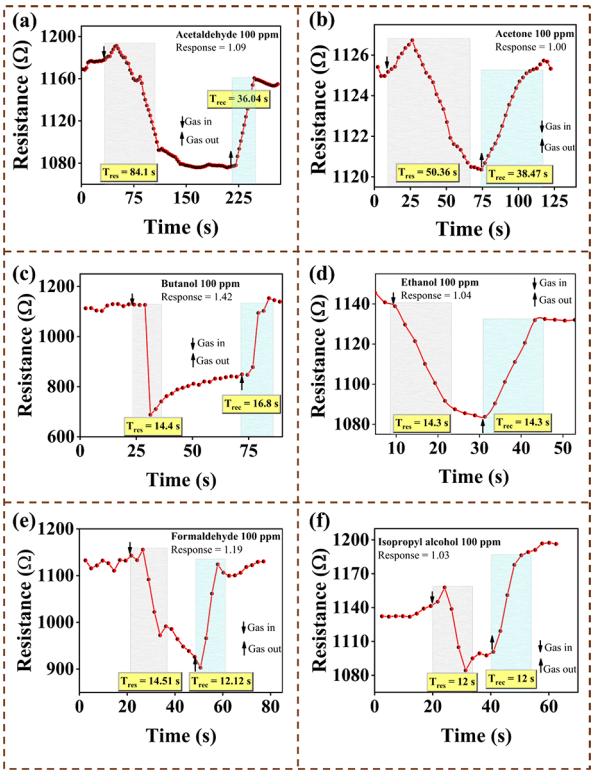

Figure 7. Sensor response of the S1 sample toward various gases at a concentration of 100 ppm: (a) acetaldehyde, (b) acetone, (c) butanol, (d) ethanol, (e) formaldehyde, and (f) formaldehyde.

demonstrates that the constructed sensor is having cross-selectivity issues. Thus, it cannot be used as a good sensor. Nevertheless, there are several reports for SnO_2 being used as a good gas sensor. However, they all were operated at high temperatures >100 °C.[14−17] The baseline resistance of the films was around 1 kΩ. This low resistance value indicates that the studied films were mesoporous and non-stoichiometric. This is because of the large amount of oxygen vacancies. The stoichiometric SnO_2 films are supposed to have resistance in the order of 10^8 Ω.[36]

The UV absorption spectra of the S1 sample give the clear picture of the intermediate sub-bands present in the forbidden gap. The fundamental bandgap was found to be 3.2 eV. There are two sub-bands present within the forbidden gap with band edges at 1.41 and 2.37 eV. This indicates that there is a weaker absorption of low-energy photons, which is primarily due to excessive defect density in SnO_2.[37] The absorption spectra and Tauc plot are given in Figure 8a,b. The individual Tauc plots for each band edge are given in the Supporting Information, Figure SI 1. Some theoretical studies are also reported for the presence of low-energy bands in S1.[38]

The electrical characteristics of the film were confirmed from the Hall effect measurements. The Hall coefficient of the film was $R_H = -0.2428$. The negative sign of R_H substantiates that the deposited S1 thin films are n-type.[39] The resistivity of the sample was $\rho = 7.13 \times 10^{-2}$ Ω cm. The sample had a high carrier concentration of $n = 2.571 \times 10^{19}$ cm^{-3} but had a poor mobility of $\mu = 3.405$ cm^2/V s. From the Hall data, the Fermi energy (E_f) and mean-free path (l) of the sample were found to be 0.115 eV and 2.049 Å, respectively, using the following equations[40]

$$E_f = \frac{h^2}{8m^*}\left(\frac{3n}{\pi}\right)^{2/3} \quad (5)$$

m^* is the effective mass of electron = 0.275 m_e[40,41]

$$l = \mu\frac{h}{2e}\left(\frac{3n}{\pi}\right)^{1/3} \quad (6)$$

It is obvious that SnO_2 is degenerate as $E_f \gg kT$ at 27 °C.[40] The FE-SEM images of the S1 sample were obtained to study the morphology, and they are given in Figure 9a,b. The sample S1 had pyramidal grains distributed uniformly over the film. From the EDX analysis, it was made clear that no other impurities were present in the sample. The grain boundaries of the pyramids were distinct and clear in the FE-SEM image. The FE-SEM images obtained at different magnifications (5 μm, 1 μm, 500 nm, and 400 nm) are given in the Supporting Information, Figure SI 2. The EDX spectrum of the S1 sample is given in Figure 10c. The color mapping of the S1 sample was obtained from the EDX analysis, from which the even distribution of Sn and O atoms over the film was confirmed. The color mapping of the S1 sample is given in the Supporting Information, Figure SI 3. The films had a rough texture. Using AFM, the root-mean-square roughness calculated for the S1 sample was 24.799 nm, which confirms the rough texture. The 2D and 3D AFM images of the S1 sample are given in Figure 10a,b.

The large carrier concentration in the sample S1 indicates the immense presence of electrons on the surface. This will hinder the change in width of the depletion region, and hence, there will be no reduction of resistance with the onset of gas. The high carrier concentration will also cause electron transfer-induced perturbations, which limit the response of the sensor.[42] Moreover, the μ and l are also lower. It is reported that higher defect density can increase scatterings and suppress the mobility. Also, small l can increase the phonon scatterings.[7] As SnO_2 thin films are polycrystalline, the grain boundaries act as trapping centers of electrons within the grains. This leads to inter- and intra-grain scattering and, consequently, low mobility.[43] Thus, high carrier concentration leads to trapping of charge carriers within the lattice sites, which hinders the carrier transport and deteriorates the electrical properties.[44] In addition, pyramidal and spherical morphologies have more grain boundary scatterings when compared to other morphologies like rods and belts. This also affected the sensor response at 27 °C. These defects are evident in the UV spectrum. At 27 °C, with the onset of target gas, the transitions occur between the valence band and defect levels. But these

https://doi.org/10.1021/acsomega.3c04038
ACS Omega 2023, 8, 32848−32854

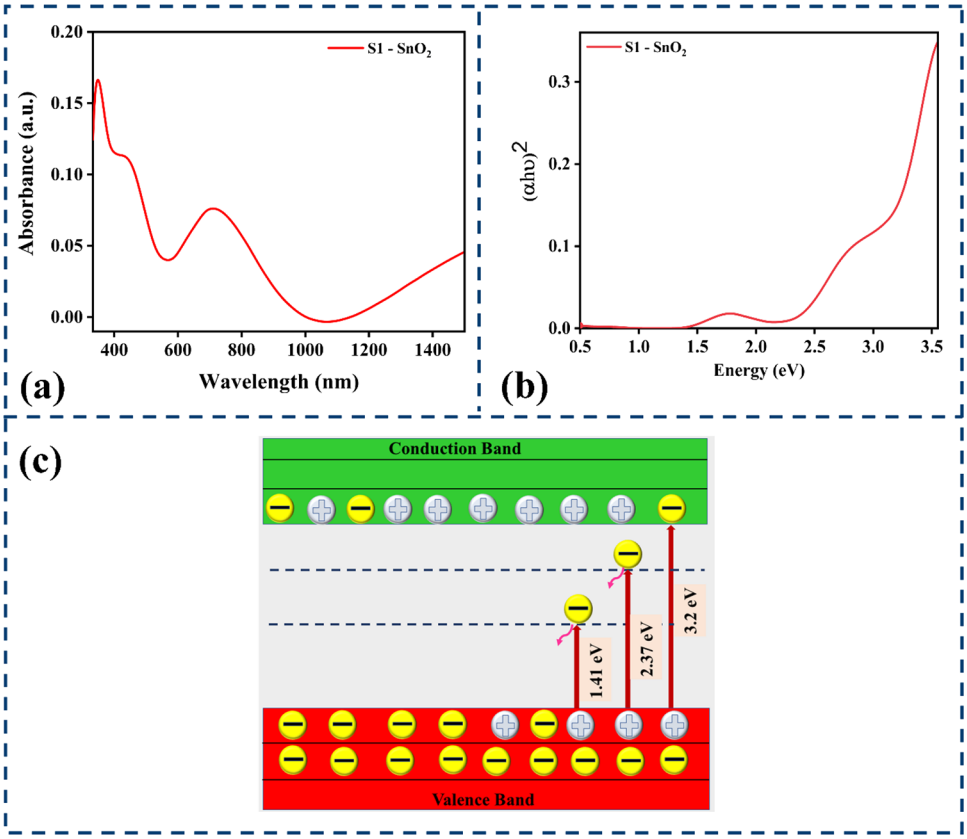

Figure 8. (a) Absorption spectra, (b) Tauc plot, and (c) schematic representation of the band structure of the SnO_2 thin film deposited at 300 °C.

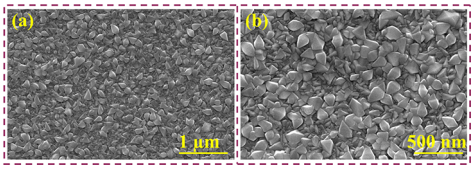

Figure 9. FE-SEM images of the SnO_2 thin film deposited at 300 °C under different magnifications: (a) 1 μm and (b) 500 nm.

electrons soon bounce back to their initial states. Thus, the electron reaching the conduction band is comparatively low. Hence, the change in resistance is significantly low, leading to a poor sensor response. In addition to this, the high potential barrier of the pristine SnO_2 bounds the number of electrons that can pass through the electron depletion region. This creates very few ionosorbed oxygen species on the surface.[42] Thus, with the onset of target gases, the surface interaction will be lower due to fewer number of oxygen ions, and so lower is the electron release and hence the low response. At higher operating temperatures, some of the defect levels will be cleared.[43] Electrons receive more energy and overcomes the scattering, and thus participates in the conduction mechanism. At high temperatures, grain boundaries reduce and enhance the mobility.[43] The potential barrier also gets reduced at high temperatures. This causes a change in depletion layer width and, correspondingly, the resistance. Thus, a good response can be achieved.

4. CONCLUSIONS

In summary, SnO_2 thin films were successfully deposited using the spray pyrolysis method. The film was uniform, compact,

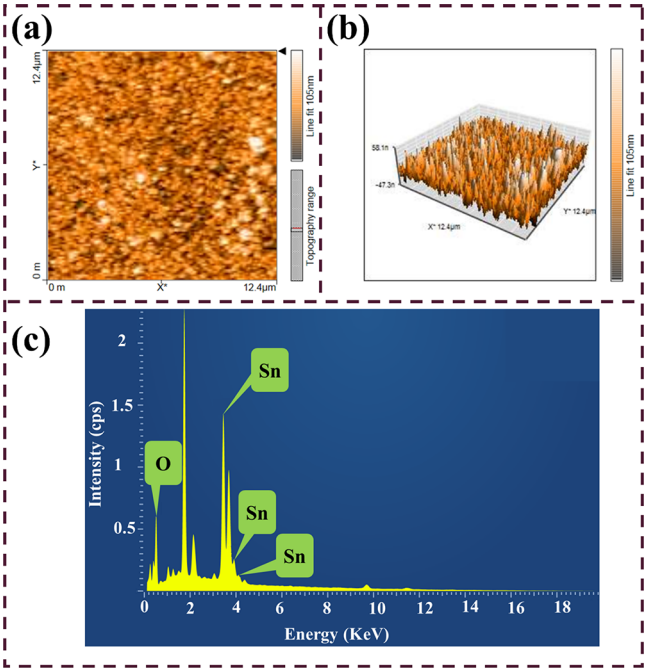

Figure 10. (a) 2D AFM image, (b) 3D AFM image, and (c) EDS spectra of the SnO_2 thin film deposited at 300 °C.

and rough. The sensor response of the film at 27 °C was poor (~1), irrespective of the gas. The low response is because of the high carrier concentration and the presence of defect levels, which give rise to scattering. The scattering at grain boundaries reduces the mobility and mean-free path of the charge carriers

https://doi.org/10.1021/acsomega.3c04038
ACS Omega 2023, 8, 32848−32854

in the semiconductor. Thus, the electrical properties and transport of carriers with the onset target gases are reduced. This leads to a poor sensor response and cross-selectivity.

■ ASSOCIATED CONTENT

Supporting Information

The Supporting Information is available free of charge at https://pubs.acs.org/doi/10.1021/acsomega.3c04038.

Tauc plots; FE-SEM images taken at different magnifications; color mapping; histograms representing the length and area of grains (PDF)

■ AUTHOR INFORMATION

Corresponding Author

Kalainathan Sivaperuman − *Centre for Nanotechnology Research, Vellore Institute of Technology, Vellore 613401, India;* orcid.org/0000-0003-2720-767X; Email: skalainathan@vit.ac.in

Authors

Anju Thomas − *School of Advanced Sciences, Vellore Institute of Technology, Vellore 632014, India;* orcid.org/0000-0002-6136-2246

Logu Thirumalaisamy − *Dept. of Physics, G.T.N Arts College (Affiliated to Madurai Kamaraj University), Madurai, Tamil Nadu 625021, India;* orcid.org/0000-0002-0802-6219

Sridharan Madanagurusamy − *Functional Nanomaterials and Devices Lab, SASTRA Deemed to be University, Thanjavur 613401, India;* orcid.org/0000-0003-4005-0507

Complete contact information is available at: https://pubs.acs.org/10.1021/acsomega.3c04038

Author Contributions

The manuscript was written through contributions of all authors. All authors have given approval to the final version of the manuscript. Conceptualization: A.T. and L.T.; formal analysis: A.T. and K.S.; investigation: A.T., L.T., and S.M.; methodology: A.T.; resources: S.M. and K.S.; supervision: K.S.; validation: L.T., S.M., and K.S.; writing of the original draft: A.T.; review and editing: A.T., L.T., S.M., and K.S.

Notes

The authors declare no competing financial interest.

■ ACKNOWLEDGMENTS

The authors would like to thank Vellore Institute of Technology and SASTRA managements for the infrastructure and characterization facilities provided for this work. A.T. would like to thank Mr. Veera Prabhu for his guidance in gas sensing.

■ REFERENCES

(1) Mounasamy, V.; Mani, G. K.; Ponnusamy, D.; Tsuchiya, K.; Prasad, A. K.; Madanagurusamy, S. Template-Free Synthesis of Vanadium Sesquioxide (V2O3) Nanosheets and Their Room-Temperature Sensing Performance. *J. Mater. Chem. A* **2018**, *6*, 6402−6413.

(2) Shendage, S. S.; Patil, V. L.; Vanalakar, S. A.; Patil, S. P.; Harale, N. S.; Bhosale, J. L.; Kim, J. H.; Patil, P. S. Sensitive and Selective NO2 Gas Sensor Based on WO3 Nanoplates. *Sens. Actuators, B* **2017**, *240*, 426−433.

(3) Yang, Y.; Ding, S.; Plovie, B.; Li, W.; Shang, C. Soft and Stretchable Electronics Design. *Encyclopedia of Sensors and Biosensors* **2023**, 258−286.

(4) Andre, R. S.; Facure, M. H. M.; Schneider, R.; Migliorini, F. L.; dos Santos, D. M.; Mercante, L. A.; Correa, D. S. Sensing Materials: Nanofibers Produced by Electrospinning and Solution Blow Spinning. *Encyclopedia of Sensors and Biosensors* **2023**, 521−541.

(5) Batzill, M.; Diebold, U. The Surface and Materials Science of Tin Oxide. *Prog. Surf. Sci.* **2005**, 47−154.

(6) Xu, X.; Liu, F.; Han, X.; Wu, Y.; Liu, W.; Zhang, R.; Zhang, N.; Wang, X. Elucidating the Promotional Effects of Niobia on SnO2 for CO Oxidation: Developing an XRD Extrapolation Method to Measure the Lattice Capacity of Solid Solutions. *Catal. Sci. Technol.* **2016**, *6*, 5280−5291.

(7) Ishibe, T.; Komatsubara, Y.; Katayama, T.; Yamashita, Y.; Naruse, N.; Mera, Y.; Hattori, A. N.; Tanaka, H.; Nakamura, Y. Interface Design of Transparent Thermoelectric Epitaxial ZnO/SnO2multilayer Film for Simultaneous Realization of Low Thermal Conductivity and High Optical Transmittance. *Appl. Phys. Lett.* **2023**, 122.

(8) Ishibe, T.; Tomeda, A.; Komatsubara, Y.; Kitaura, R.; Uenuma, M.; Uraoka, Y.; Yamashita, Y.; Nakamura, Y. Carrier and Phonon Transport Control by Domain Engineering for High-Performance Transparent Thin Film Thermoelectric Generator. *Appl. Phys. Lett.* **2021**, 118.

(9) Yu, S.; Li, L.; Xu, D.; Dong, H.; Jin, Y. Characterization of SnO2/Cu/SnO2 Multilayers for High Performance Transparent Conducting Electrodes. *Thin Solid Films* **2014**, *562*, 501−505.

(10) Yu, S.; Zhang, W.; Li, L.; Xu, D.; Dong, H.; Jin, Y. Transparent Conductive Sb-Doped SnO2/Ag Multilayer Films Fabricated by Magnetron Sputtering for Flexible Electronics. *Acta Mater.* **2013**, *61*, 5429−5436.

(11) Xu, X.; Zhang, R.; Zeng, X.; Han, X.; Li, Y.; Liu, Y.; Wang, X. Effects of La, Ce, and Y Oxides on SnO2 Catalysts for CO and CH4 Oxidation. *ChemCatChem* **2013**, *5*, 2025−2036.

(12) Zhao, R.; Wang, Z.; Yang, Y.; Xing, X.; Zou, T.; Wang, Z.; Wang, Y. Raspberry-like SnO2 Hollow Nanostructure as a High Response Sensing Material of Gas Sensor toward n-Butanol Gas. *J. Phys. Chem. Solids* **2018**, *120*, 173−182.

(13) Kong, Y.; Li, Y.; Cui, X.; Su, L.; Ma, D.; Lai, T.; Yao, L.; Xiao, X.; Wang, Y. SnO2 Nanostructured Materials Used as Gas Sensors for the Detection of Hazardous and Flammable Gases: A Review. *Nano Mater. Sci.* **2022**, *4*, 339−350.

(14) Bose, K.; Kesavan, R.; Deepa, S. Effect of Dysprosium Doping on the Structural and Gas Sensing Properties of SnO2 Thin Films. In *AIP Conference Proceedings*; American Institute of Physics Inc., 2020; Vol. *2263*, DOI: 10.1063/5.0017283.

(15) Deepa, S.; George, A. S. Effect of Microwave Irradiation on the Gas Sensing Properties of SnO2 Thin Films. *Mater. Today: Proc.* **2020**, *33*, 2228−2232.

(16) Kolhe, P. S.; Kulkarni, S. G.; Maiti, N.; Sonawane, K. M. Effect of Cu Doping Concentration on H2S Gas-Sensing Properties of Cu-Doped SnO2 Thin Films. *Appl. Phys. A: Mater. Sci. Process.* **2019**, 125.

(17) Lackner, E.; Krainer, J.; Wimmer-Teubenbacher, R.; Sosada, F.; Deluca, M.; Gspan, C.; Rohracher, K.; Wachmann, E.; Köck, A. Carbon Monoxide Detection with CMOS Integrated Thin Film SnO2 Gas Sensor. In *Materials Today: Proceedings*; Elsevier Ltd, 2017; Vol. *4*, pp. 7128−7131, DOI: 10.1016/j.matpr.2017.08.007.

(18) Eisele, I.; Doll, T.; Burgmair, M. Low Power Gas Detection with FET Sensors. *Sens. Actuators, B* **2001**, *78*, 19−25.

(19) Gorup, L. F.; Amorin, L. H.; Camargo, E. R.; Sequinel, T.; Cincotto, F. H.; Biasotto, G.; Ramesar, N.; La Porta, F. D. A. *Methods for Design and Fabrication of Nanosensors: The Case of ZnO-Based Nanosensor*. In Nanosensors for Smart Cities; Elsevier, 2020; pp. 9−30, DOI: 10.1016/b978-0-12-819870-4.00002-5.

(20) Korotcenkov, G.; Han, S. D.; Cho, B. K.; Brinzari, V. Grain Size Effects in Sensor Response of Nanostructured SnO2- and In2O3-Based Conductometric Thin Film Gas Sensor. *Crit. Rev. Solid State Mater. Sci.* **2009**, *34*, 1−17.

(21) Ravikumar, T.; Thirumalaisamy, L.; Madanagurusamy, S.; Sivaperuman, K. Substrate Temperature Dependent Ammonia Gas Sensing Performance of Zinc Ferrite Thin Films Prepared by Spray Pyrolysis Technique. *J. Alloys Compd.* **2023**, *959*, No. 170568.
(22) Yunusa, Z.; Hamidon, M. N.; Awang, Z.; Kaiser, A.; Awang, Z. Gas Sensors: A Review. *Sens. Transducers* **2014**, *168*, 61−75.
(23) Cho, B.; Kim, J. Toluene Sensing Characteristics of Tin Oxide-Based Gas Sensor Deposited with Various Amounts of Metal-loporphyrin. *Micro-Nano Syst. Lett.* **2022**, *10*, 3.
(24) Onofre, Y. J.; Catto, A. C.; Bernardini, S.; Fiorido, T.; Aguir, K.; Longo, E.; Mastelaro, V. R.; da Silva, L. F.; de Godoy, M. P. F. Highly Selective Ozone Gas Sensor Based on Nanocrystalline Zn 0.95 Co 0.05 O Thin Film Obtained via Spray Pyrolysis Technique. *Appl. Surf. Sci.* **2019**, *478*, 347−354.
(25) Mani, G. K.; Rayappan, J. B. B. Novel and Facile Synthesis of Randomly Interconnected ZnO Nanoplatelets Using Spray Pyrolysis and Their Room Temperature Sensing Characteristics. *Sens. Actuators, B* **2014**, *198*, 125−133.
(26) Pandeeswari, R.; Jeyaprakash, B. G. High Sensing Response of β-Ga2O3 Thin Film towards Ammonia Vapours: Influencing Factors at Room Temperature. *Sens. Actuators, B* **2014**, *195*, 206−214.
(27) Nallakumar, S.; Thirumalaisamy, L.; Madhanagurusamy, S.; Kalainathan, S.; Usha Rani, M. Inverse and Distorted Co_2 SnO_4 Cubic Spinel Thin Films for Dimethylamine Detection at Room Temperature. *New J. Chem.* **2023**, *47*, 11110−11122.
(28) Zhao, J.; Huo, L. H.; Gao, S.; Zhao, H.; Zhao, J. G. Alcohols and Acetone Sensing Properties of SnO2 Thin Films Deposited by Dip-Coating. *Sens. Actuators, B* **2006**, *115*, 460−464.
(29) Nurfani, E.; Lailani, A.; Kesuma, W. A. P.; Anrokhi, M. S.; Kadja, G. T. M.; Rozana, M. UV Sensitivity Enhancement in Fe-Doped ZnO Films Grown by Ultrafast Spray Pyrolysis. *Opt. Mater. (Amst)* **2021**, 112.
(30) Eqbal, E.; Anila, E. I. Tailoring the Properties of Tin Dioxide Thin Films by Spray Pyrolysis Technique. *Opt. Mater. (Amst)* **2021**, 122.
(31) Ghorannevis, Z.; Hosseinnejad, M. T.; Habibi, M.; Golmahdi, P. Effect of Substrate Temperature on Structural, Morphological and Optical Properties of Deposited Al/ZnO Films. *J. Theor. Appl. Phys.* **2015**, *9*, 33−38.
(32) Daouahi, M.; Rekik, N. Effect of Substrate Temperature on (Micro/Nano)Structure of a-SiC:H Thin Films Deposited by Radio-Frequency Magnetron Sputtering. *J. Phys. Chem. C* **2012**, *116*, 21018−21026.
(33) Jain, N.; Kumawat, R.; Sharma, S. K. Effect of Substrate Temperature on the Microstructural and Optical Properties of RF Sputtered Grown ZnO Thin Films. In *Materials Today: Proceedings*; Elsevier Ltd, 2020; Vol. *30*, pp. 93−99, DOI: 10.1016/j.matpr.2020.04.667.
(34) Mäki-Jaskari, M. A.; Rantala, T. T. Band Structure and Optical Parameters of the SnO2(110) Surface. *Phys. Rev. B* **2001**, *64*, No. 075407.
(35) Abee, M. W.; Cox, D. F. BF3 Adsorption on Stoichiometric and Oxygen-Deficient SnO2(110) Surfaces. *J. Phys. Chem. B* **2003**, *107*, 1814−1820.
(36) Haddad, K.; Abokifa, A.; Kavadiya, S.; Lee, B.; Banerjee, S.; Raman, B.; Banerjee, P.; Lo, C.; Fortner, J.; Biswas, P. SnO2 Nanostructured Thin Films for Room-Temperature Gas Sensing of Volatile Organic Compounds. *ACS Appl. Mater. Interfaces* **2018**, *10*, 29972−29981.
(37) Lee, S.; Kim, S.; Shin, S.; Jin, Z.; Min, Y. S. Band Structure of Amorphous Zinc Tin Oxide Thin Films Deposited by Atomic Layer Deposition. *J. Ind. Eng. Chem.* **2018**, *58*, 328−333.
(38) Arlinghaus, F. J. *ENERGY BANDS IN STANNIC OXIDE (SnO2)*; Pergamon Press, 1974; Vol. *35*.
(39) Farahi, N.; Prabhudev, S.; Botton, G. A.; Salvador, J. R.; Kleinke, H. Nano- and Microstructure Engineering: An Effective Method for Creating High Efficiency Magnesium Silicide Based Thermoelectrics. *ACS Appl. Mater. Interfaces* **2016**, *8*, 34431−34437.
(40) Babar, A. R.; Shinde, S. S.; Moholkar, A. V.; Bhosale, C. H.; Rajpure, K. Y. Structural and Optoelectronic Properties of Sprayed Sb:SnO2 Thin Films: Effects of Substrate Temperature and Nozzle-to-Substrate Distance. *J. Semicond.* **2011**, *32*, No. 102001.
(41) Button, J. K.; Fonstad, C. G.; Dreybrodt, W. Determination of the Electron Masses in Stannic Oxide by Submillimeter Cyclotron Resonance. *Phys. Rev. B* **1971**, *4*, 4539.
(42) Xu, K.; Li, N.; Zeng, D.; Tian, S.; Zhang, S.; Hu, D.; Xie, C. Interface Bonds Determined Gas-Sensing of SnO2-SnS2 Hybrids to Ammonia at Room Temperature. *ACS Appl. Mater. Interfaces* **2015**, *7*, 11359−11368.
(43) Zhu, Y.; Yu, M.; Lv, Q.; Hou, H.; Yang, J.; Liu, G.; Liu, J.; Qiao, G. Effects of the High-Temperature Sensitization in Argon Atmosphere on the Microstructure and Properties of Polycrystalline PbSe Films. *Mater. Sci. Semicond. Process.* **2023**, 162.
(44) Sankarasubramanian, K.; Soundarrajan, P.; Logu, T.; Sethuraman, K.; Ramamurthi, K. Enhancing Resistive-Type Hydrogen Gas Sensing Properties of Cadmium Oxide Thin Films by Copper Doping. *New J. Chem.* **2018**, *42*, 1457−1466.
(45) Adachi, N.; Hisatomi, T.; Sano, M.; Tsuya, H. Reduction of Grown-In Defects by High Temperature Annealing. *J. Electrochem. Soc.* **2000**, *147*, 350.

https://doi.org/10.1021/acsomega.3c04038
ACS Omega 2023, 8, 32848−32854